ChemComm

Check for updates

ROYAL SOCIETY
OF CHEMISTRY

Monitoring mitochondrial nitroreductase activity in tumors and a hind-limb model of ischemia in mice using a novel activatable NIR fluorescent probe†

Xiaosheng Liu,‡[a] Shuang Zeng,‡[a] Ming Zhang,[a] Maojun Jiang,[b] Yves S. Kafuti,[a] Pingping Shangguan,[a] Yichu Yu,[a] Qixian Chen, [iD][a] Jingyun Wang, [iD] *[ab] Xiaojun Peng, [iD][b] Juyoung Yoon [iD] *[c] and Haidong Li [iD] *[ab]

We report a mitochondria-targeted nitroreductase (NTR)-activated near-infrared fluorescent probe: $CS-NO_2$. Overexpressed NTR in mitochondria was measured with high sensitivity. More importantly, the probe $CS-NO_2$ successfully monitored NTR activity in solid tumors and a hind-limb model of ischemia in mice. This novel finding indicates the promising function of our probe for the diagnosis of solid tumors and hypoxia-associated diseases.

Solid tumors are distinguished by their hypoxic microenvironment, which results from an unbalanced relationship between oxygen delivery and oxygen uptake. Indeed, 50% to 60% of solid tumors that show locally progression have an uneven distribution of hypoxia.[1,2] A hypoxic microenvironment can stimulate epithelial–mesenchymal transition, promote angiogenesis, and increase the risk of tumor metastasis.[3,4] Tumors in a hypoxic microenvironment become more aggressive under metabolic stress, inhibit anti-tumor immunity, and reduce chemosensitivity, thereby hindering treatment.[5–10] Moreover, hypoxia is associated intimately with inflammation and organ damage.[11–13] Thus, detection of a hypoxic microenvironment is crucial for the diagnosis, monitoring, and cure of cancers and several other disorders.[14,15]

Traditional medical-imaging methods, such as magnetic resonance imaging, computed tomography, and positron emission tomography, are challenging to use when diagnosing cancer at the molecular level. Methods based on fluorescence imaging are utilized extensively for disease diagnosis and detection of physiological processes at cellular, tissue, and molecular levels and in live organisms because of their non-invasiveness, strong biocompatibility, and high spatial and temporal resolution.[16–18] Near-infrared (NIR) fluorescence allows deep penetration of tissue and little interference, and could be applied for clinical use.[19–24]

Nitroreductases (NTRs) are flavin-containing enzymes. They can reduce nitro compounds if nicotinamide adenine dinucleotide (NADH) is used as an electron donor. NTRs can be divided into types I and II based on whether or not the catalytic reaction is sensitive to oxygen.[25–27] An increased NTR level is a biomarker of tumor cells.[25–27] Type-I NTRs have been detected in cancer cells incubated under normoxia.[28] However, most probes used for cancer diagnoses based on the NTR response are activated in hypoxic cancer cells, which suggests that NTRs exist mainly in the oxygen-sensitive form (type II) in hypoxic cancer cells.[29] The reduction mechanism of type-II NTRs involves continuous transfer of single electrons, and mitochondria are the main sites for redox reactions in eukaryotes.[30–32] Therefore, we suspect that type-II NTR-catalyzed reductions take place in hypoxic mitochondria. However, most fluorescent probes dependent on NTR activation lack the capacity to target organelles. Also, monitoring NTR activity in a subcellular structure under a hypoxic microenvironment is difficult (especially in mitochondria).[33–37] In addition, oxygen in cells is consumed mainly in the mitochondrial respiratory chain, and the structure and function of mitochondria in a hypoxic microenvironment will be affected.[38,39] Studies have shown that hypoxia can affect the morphological changes of mitochondria, causing changes in the composition of the electron transport chain (ETC) complex. Such changes reshape the ETC and reduce the activity of the tricarboxylic acid cycle to adapt to hypoxia, and mitochondrial metabolic pathways and hypoxia-inducible factor (HIF) pathways carry out crosstalk under hypoxia.[40] Therefore, tracking and labeling mitochondria in cancer cells is important for the study of cellular metabolic pathways under hypoxia.

[a] School of Bioengineering, Dalian University of Technology, 2 Linggong Road, Hi-tech Zone, Dalian 116024, China. E-mail: wangjingyun67@dlut.edu.cn, lihd@dlut.edu.cn

[b] State Key Laboratory of Fine Chemicals, Frontiers Science Center for Smart Materials Oriented Chemical Engineering, Dalian University of Technology, 2 Linggong Road, Hi-tech Zone, Dalian 116024, China

[c] Department of Chemistry and Nanoscience, Ewha Womans University, 52 Ewhayeodae-gil, Seodaemun-gu, Seoul 03760, Korea. E-mail: jyoon@ewha.ac.kr

† Electronic supplementary information (ESI) available. See DOI: https://doi.org/10.1039/d2cc04112j

‡ These authors contributed equally.
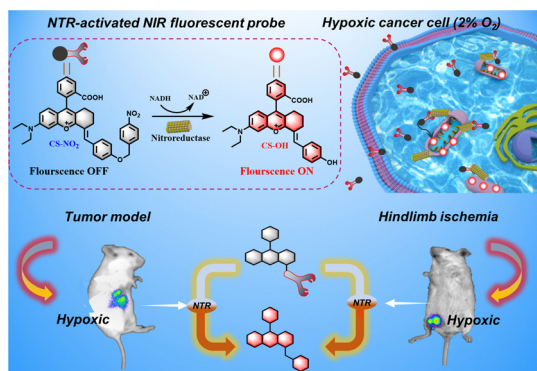
Scheme 1 The activation of the mitochondria-targeting probe **CS-NO₂** by nitroreductase (NTR), the utilization of the probe **CS-NO₂** for visualizing tumors, and its use in a hind-limb model of ischemia in mice.

We developed and synthesized a mitochondrial-targeted NIR fluorescent probe, **CS-NO₂**, for localization of mitochondria in hypoxic cells. We applied this probe in a mouse model of solid tumors and hind-limb ischemia (Scheme 1). Rhodamine is a water-soluble cationic dye that can be inserted into mitochondria through the mitochondrial membrane potential.[41–44] By expanding the conjugated structure of rhodamine B, we obtained the NIR-fluorescence group **CS-OH**. We introduced *p*-nitrobenzyl as the recognition site of NTR to produce **CS-NO₂**. We quenched fluorescence emission by inhibiting intramolecular charge transfer. The nitro unit in **CS-NO₂** was reduced by NTR to an amino motif in the presence of NADH. This action was followed by 1,6-self-elimination, which released a free **CS-OH** with intense fluorescence (Fig. S10, ESI†) for hypoxia imaging *in vitro* and *in vivo*.

The response of **CS-NO₂** (10 μM) to NTR (10 μg mL⁻¹) in a HEPES buffer system (pH 7.4; 10% DMSO) was studied. Absorbance at 580 nm increased significantly (Fig. 1A), and the solution changed from colourless to purple after the probe **CS-NO₂** had been incubated with NTR. Accordingly, the fluorescence intensity at 670 nm of **CS-NO₂** increased significantly after incubation with NTR (Fig. 1B) in the presence of NADH, and the fluorescence quantum yield (Φ_f) increased from 0.52% to 10.38%. We verified the activation process of **CS-NO₂** stated above by high-resolution mass spectrometry (Fig. S11, ESI†).
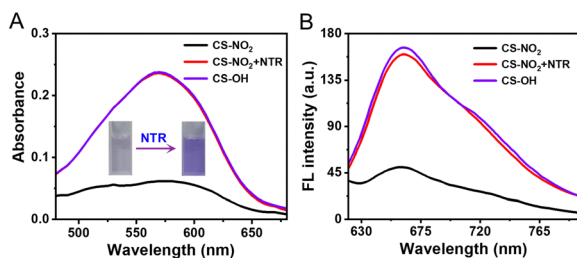
Selectivity assessment of **CS-NO₂** to NTR was carried out to further verify that **CS-NO₂** produces a specific response during biomonitoring. The fluorescence changes of **CS-NO₂** with various potential-interfering species found commonly in organisms were investigated under identical conditions. A significant fluorescence increase was not detected with **CS-NO₂** upon exposure to potential interfering species (Fig. 2A). When **CS-NO₂** was incubated only with NTR (10 μg mL⁻¹) and NADH (0.5 mM), the fluorescence intensity increased sharply, indicating that **CS-NO₂** had excellent selectivity for NTR: this feature is extremely beneficial for monitoring of hypoxic regions *in vivo*.

Next, we tested the time-dependent response of the probe **CS-NO₂** (10 μM) to NTR (10 μg mL⁻¹). The absorbance and fluorescence intensity of the reaction system was measured at different incubation times using a UV-vis spectrophotometer and fluorescence spectrometer. With an increase in incubation time, the fluorescence and absorbance changed (Fig. 2B and Fig. S12A, ESI†) and reached a *plateau* in ~1 h (Fig S13, ESI†), These data suggested the sensitivity of **CS-NO₂** to NTR.

Moreover, the sensing behavior of probe **CS-NO₂** (10 μM) to various equivalents of NTR (0–4 μg mL⁻¹) was tested. The maximum fluorescence intensity and absorbance of **CS-NO₂** increased as the NTR dose increased (Fig. 2C and Fig. S12B, ESI†). In an NTR concentration range of 0–1.2 μg mL⁻¹ (Fig. 2D), the connection between the emission intensity of **CS-NO₂** and NTR dose was linear, with a linear correlation coefficient of 0.9758. These data indicated that **CS-NO₂** could be used to detect NTR *in vitro*.

We wished to further understand the possible interaction between our probe and enzymes and the catalytic mechanism of NTR. We used Auto-Dock tools to calculate docking. The crystal structure of NTR from the PDB database (PDB code:
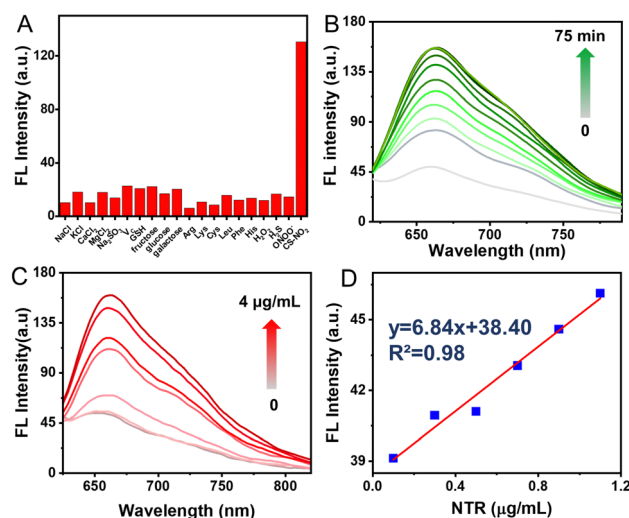
Fig. 2 Spectral characteristics of **CS-NO₂** (10 μM) with respect to nitroreductase (NTR). (A) The fluorescence response of **CS-NO₂** to various species. (B) Time-dependent changes in the fluorescence emission of **CS-NO₂** in the presence of NTR (10 μg mL⁻¹). (C) Fluorescence responses of **CS-NO₂** to NTR (0–4 μg mL⁻¹) after incubation for 1 h at 37 °C. (D) The linear connection between the NTR (0–1.2 μg mL⁻¹) concentration and fluorescence intensity (670 nm). λ_{ex} = 580 nm.

Fig. 1 After 1 h of incubation at 37 °C, the (A) absorption and (B) fluorescence spectra of **CS-NO₂** (10 μM) in the absence and presence of NTR (10 μg mL⁻¹) with NADH (0.5 mM). λ_{ex} = 580 nm. Inset of (A): visible-light images of **CS-NO₂** in the absence and presence of NTR.
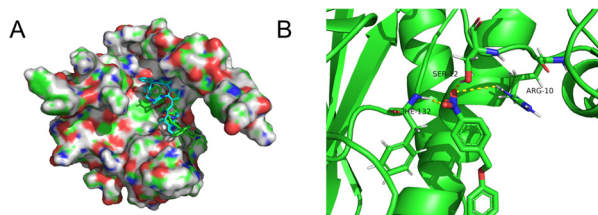
Fig. 3 (A) Calculated binding model of **CS-NO₂** with NTR. (B) The hydrogen bonds between **CS-NO₂** and amino-acid residues (Phe-132, Ser-12, and Arg-10) in NTR.

4DN2) was selected as the research model. **CS-NO₂** could fit into the hydrophobic cavity of an enzyme due to hydrophobic interactions with the NTR protein and aromatic π–π interactions (Fig. 3A). In addition, the ribbon-band model established by Pymol showed that the oxygen atom of the nitro group of **CS-NO₂** could form three hydrogen bonds with the amino-acid residues (Phe-132, Ser-12 and Arg-10) of NTR. These hydrogen bonds anchored **CS-NO₂** firmly to NTR (Fig. 3B).

Before cell imaging, the biological compatibility of **CS-NO₂** was detected using the MTT assay (Fig. S14, ESI†). This showed that **CS-NO₂** had weak toxicity to 4T1 cells and MCF-7 cells, and was an appropriate probe for NTR detection in live cells.

The sensing ability of **CS-NO₂** to NTR was tested in 4T1 cells and MCF-7 cells incubated in a hypoxic environment (Fig. 4A and Fig. S15, ESI†). After 8 h of incubation under hypoxia (2% O_2), 4T1 cells showed obvious red fluorescence, whereas cells incubated in a normal environment did not show fluorescence. After incubation in a hypoxic environment and treatment with the NTR inhibitor dicumarol, the red fluorescence disappeared. These data further validated the selectivity of **CS-NO₂** to NTR in cells. HIF-α is not expressed in normal cells, and it can be expressed stably only under hypoxic conditions. Expression of this protein is positively correlated with the degree of cell hypoxia. To further evaluate the hypoxia of cells under two culture conditions, we measured expression of HIF-1α protein by immunofluorescence staining and compared it with the confocal fluorescence microscopy of probe **CS-NO₂**. The opening and closing of the immunofluorescence channel and NIR fluorescence channel of the probe were synchronous. These data verified the specificity of probe opening under hypoxia, and indicated that activation of probe **CS-NO₂** was caused by type-II NTR (oxygen-sensitive) catalysis. To investigate the location of this probe further, we used confocal fluorescence microscopy to study the distribution of intensity in cells (Fig. 4B and Fig. S16, ESI†). First, we used the commercial organelle-targeting dyes Mito-Tracker™ Green, Lyso-Tracker™ Green, ER-Tracker™ Green, and Hoechst 33342 to pre-label mitochondria, endoplasmic reticula, lysosomes, and nuclei in cells, respectively, and then undertook co-incubation with **CS-NO₂**. Through co-localization analyses of probe **CS-NO₂** with different dyes, the Pearson's colocalization coefficient used to describe the intensity distribution between the two channels was calculated to be 0.9116, 0.6185, 0.4724, and 0.0274, for Mito-Tracker Green, Lyso-Tracker Green, ER-Tracker Green, and Hoechst 33342, respectively. These results showed that probe **CS-NO₂** could locate the mitochondria of hypoxic cells specifically. Most of the NTR-based fluorescent probes reported so far can be used only to monitor cellular hypoxia: few fluorescent probes can also label mitochondria selectively.

Due to the high sensitivity and specificity of **CS-NO₂** to NTR, a tumor-bearing model and hind-limb ischemic model in mice was used to test the capability of probe **CS-NO₂** to monitor NTR *in vivo*. Both models showed enhanced fluorescence signals over time (Fig. 5). Compared with the control group (phosphate-buffered saline), probe **CS-NO₂** distinguished the tumor or hind-limb-operation site from surrounding normal tissue within 45 min upon local injection. These findings implied that **CS-NO₂** could be used as a NIR fluorescent probe in the monitoring of solid-tumor markers and other hypoxia-related diseases.

In conclusion, we designed and synthesized a rhodamine-based fluorescent probe for sensing endogenous NTR activity. The reactive probe **CS-NO₂**, quenched by the *p*-nitrobenzyl group, had high selectivity and sensitivity. The specific response
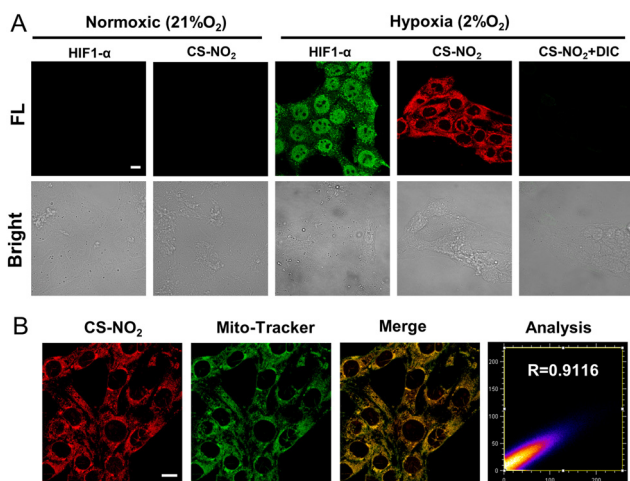

Fig. 4 (A) Immunofluorescence imaging of the expression of HIF-1α protein and confocal fluorescence microscopy imaging of 4T1 cells treated under various circumstances with **CS-NO₂**. Scale bar: 10 μm. (B) Co-localization of **CS-NO₂** (red, λ_{ex} = 580 nm, λ_{em} = 600–700 nm) and commercial mitochondrial dye (green, λ_{ex} = 488 nm, λ_{em} = 510–530 nm) for organelles in 4T1 cells. Scale bar: 10 μm.

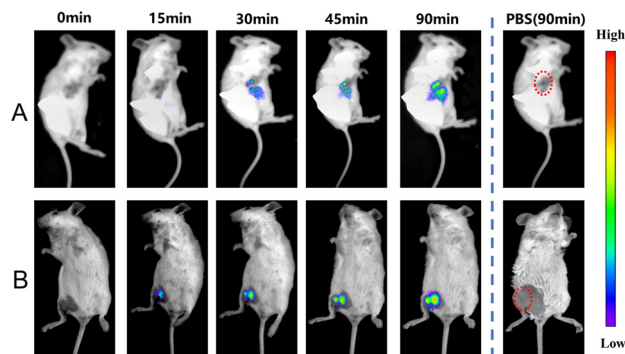**Fig. 5** *In vivo* fluorescence imaging of hypoxia in mice (A) bearing tumors and with (B) hind-limb ischemia. λ_{ex} = 550 nm, λ_{em} = 760 nm.

of NTR to **CS-NO₂** was verified *via* spectroscopic characterization and molecular docking analysis. Imaging of cell lines (4T1 and MCF-7) under hypoxia further verified the excellent monitoring ability of the probe **CS-NO₂** towards endogenous NTR activity. More importantly, **CS-NO₂** could target mitochondria selectively, thereby providing a potent instrument for researching the metabolism of nitro compounds in cells under hypoxia. **CS-NO₂** could monitor hypoxic regions in a tumor-bearing mouse model. It could also distinguish hypoxic regions in normal tissues and surgical sites in a hind-limb model of ischemia in mice; this has not been demonstrated before. This efficient NIR fluorescent probe may provide a new strategy for diagnosing and monitoring hypoxia-related diseases.

Conflicts of interest

There are no conflicts to declare.

Notes and references

1 S. B. Bader, M. W. Dewhirst and E. M. Hammond, *Cancers*, 2020, **13**, 27.
2 Y. Li, Y. Sun, J. Li, Q. Su, W. Yuan, Y. Dai, C. Han, Q. Wang, W. Feng and F. Li, *J. Am. Chem. Soc.*, 2015, **137**, 6407–6416.
3 A. L. Harris, *Nat. Rev. Cancer*, 2002, **2**, 38–47.
4 J. P. Joseph, M. K. Harishankar, A. A. Pillai and A. Devi, *Oral Oncol.*, 2018, **80**, 23–32.
5 S. K. Daniel, K. M. Sullivan, K. P. Labadie and V. G. Pillarisetty, *Clin. Transl. Med.*, 2019, **8**, 10.
6 C. Riera-Domingo, A. Audige, S. Granja, W. C. Cheng, P. C. Ho, F. Baltazar, C. Stockmann and M. Mazzone, *Physiol. Rev.*, 2020, **100**, 1–102.
7 N. E. Scharping, D. B. Rivadeneira, A. V. Menk, P. D. A. Vignali, B. R. Ford, N. L. Rittenhouse, R. Peralta, Y. Wang, Y. Wang, K. DePeaux, A. C. Poholek and G. M. Delgoffe, *Nat. Immunol.*, 2021, **22**, 205–215.
8 J. Tao, G. Yang, W. Zhou, J. Qiu, G. Chen, W. Luo, F. Zhao, L. You, L. Zheng, T. Zhang and Y. Zhao, *J. Hematol. Oncol.*, 2021, **14**, 14.
9 B. Wang, Q. Zhao, Y. Zhang, Z. Liu, Z. Zheng, S. Liu, L. Meng, Y. Xin and X. Jiang, *J. Exp. Clin. Cancer Res.*, 2021, **40**, 24.
10 Y. Yang, X. Liu, W. Ma, Q. Xu, G. Chen, Y. Wang, H. Xiao, N. Li, X. J. Liang, M. Yu and Z. Yu, *Biomaterials*, 2021, **265**, 120456.
11 A. Emami Nejad, S. Najafgholian, A. Rostami, A. Sistani, S. Shojaeifar, M. Esparvarinha, R. Nedaeinia, S. Haghjooy Javanmard, M. Taherian, M. Ahmadlou, R. Salehi, B. Sadeghi and M. Manian, *Cancer Cell Int.*, 2021, **21**, 62.
12 S. Konisti, S. Kiriakidis and E. M. Paleolog, *Nat. Rev. Rheumatol.*, 2012, **8**, 153–162.
13 J. W. Lee, J. Ko, C. Ju and H. K. Eltzschig, *Exp. Mol. Med.*, 2019, **51**, 1–13.
14 J. Sun, Z. Hu, R. Wang, S. Zhang and X. Zhang, *Anal. Chem.*, 2019, **91**, 1384–1390.
15 X. Zhao, S. Long, M. Li, J. Cao, Y. Li, L. Guo, W. Sun, J. Du, J. Fan and X. Peng, *J. Am. Chem. Soc.*, 2020, **142**, 1510–1517.
16 H. Li, Q. Yao, W. Sun, K. Shao, Y. Lu, J. Chung, D. Kim, J. Fan, S. Long, J. Du, Y. Li, J. Wang, J. Yoon and X. Peng, *J. Am. Chem. Soc.*, 2020, **142**, 6381–6389.
17 J. Yin, L. Huang, L. Wu, J. Li, T. D. James and W. Lin, *Chem. Soc. Rev.*, 2021, **50**, 12098–12150.
18 Y. Zhang, G. Zhang, Z. Zeng and K. Pu, *Chem. Soc. Rev.*, 2022, **51**, 566–593.
19 H. Li, Q. Yao, J. Fan, N. Jiang, J. Wang, J. Xia and X. Peng, *Chem. Commun.*, 2015, **51**, 16225–16228.
20 H. Li, H. Kim, F. Xu, J. Han, Q. Yao, J. Wang, K. Pu, X. Peng and J. Yoon, *Chem. Soc. Rev.*, 2022, **51**, 1795–1835.
21 H. Li, Y. Li, Q. Yao, J. Fan, W. Sun, S. Long, K. Shao, J. Du, J. Wang and X. Peng, *Chem. Sci.*, 2019, **10**, 1619–1625.
22 J. Mu, M. Xiao, M. Shi, X. Geng, H. Li, Y. Yin and X. Chen, *Angew. Chem., Int. Ed.*, 2022, **61**, e202114722.
23 M. Ling, R. Sun, G. Li, M. Z. Syeda, W. Ma, Z. Mai, L. Shao, L. Tang and Z. Yu, *Nano Res.*, 2022, **15**, 6288–6296.
24 Z. Wang, L. Yu, Y. Wang, C. Wang, Q. Mu, X. Liu, M. Yu, K. N. Wang, G. Yao and Z. Yu, *Adv. Sci.*, 2022, **9**, e2104793.
25 S. Chen, J. Liu, Y. Li, X. Wu, Q. Yuan, R. Yang and J. Zheng, *TrAC, Trends Anal. Chem.*, 2020, **131**, 116010.
26 X. Meng, F. Yang, H. Dong, L. Dou and X. Zhang, *Nano Today*, 2021, **38**, 101156.
27 H. Zhou, M. Guo, J. Li, F. Qin, Y. Wang, T. Liu, J. Liu, Z. F. Sabet, Y. Wang, Y. Liu, Q. Huo and C. Chen, *J. Am. Chem. Soc.*, 2021, **143**, 1846–1853.
28 A. Chevalier, Y. Zhang, O. M. Khdour, J. B. Kaye and S. M. Hecht, *J. Am. Chem. Soc.*, 2016, **138**, 12009–12012.
29 H. Li, D. Kim, Q. Yao, H. Ge, J. Chung, J. Fan, J. Wang, X. Peng and J. Yoon, *Angew. Chem., Int. Ed.*, 2021, **60**, 17268–17289.
30 M. Khacho, R. Harris and R. S. Slack, *Nat. Rev. Neurosci.*, 2019, **20**, 34–48.
31 E. M. Williams, R. F. Little, A. M. Mowday, M. H. Rich, J. V. Chan-Hyams, J. N. Copp, J. B. Smaill, A. V. Patterson and D. F. Ackerley, *Biochem. J.*, 2015, **471**, 131–153.
32 M. Zhu, R. R. Liu, H. L. Zhai, Y. J. Meng, L. Han and C. L. Ren, *Int. J. Biol. Macromol.*, 2020, **150**, 509–518.
33 M. Li, Y. Zhang, X. Ren, W. Niu, Q. Yuan, K. Cao, J. Zhang, X. Gao and D. Su, *Chem. Commun.*, 2022, **58**, 819–822.
34 W. Qin, C. Xu, Y. Zhao, C. Yu, S. Shen, L. Li and W. Huang, *Chin. Chem. Lett.*, 2018, **29**, 1451–1455.
35 X. Wu, W. Shi, X. Li and H. Ma, *Acc. Chem. Res.*, 2019, **52**, 1892–1904.
36 F. Xu, M. Fan, S. Kang and X. Duan, *Anal. Chim. Acta*, 2019, **1088**, 131–136.
37 S. Zhang, H. Chen, L. Wang, X. Qin, B. P. Jiang, S. C. Ji, X. C. Shen and H. Liang, *Angew. Chem., Int. Ed.*, 2022, **61**, e202107076.
38 R. A. Smith, R. C. Hartley, H. M. Cocheme and M. P. Murphy, *Trends Pharmacol. Sci.*, 2012, **33**, 341–352.
39 Z. Yang, J. Wang, S. Liu, X. Li, L. Miao, B. Yang, C. Zhang, J. He, S. Ai and W. Guan, *Biomaterials*, 2020, **229**, 119580.
40 D. C. Fuhrmann and B. Brune, *Redox. Biol.*, 2017, **12**, 208–215.
41 X. Jing, F. Yang, C. Shao, K. Wei, M. Xie, H. Shen and Y. Shu, *Mol. Cancer*, 2019, **18**, 157.
42 Z. Mi, L. Liu, Y. Zhao and J. Guan, *Int. J. Biol. Macromol.*, 2020, **164**, 932–938.
43 L. Yuan, W. Lin, K. Zheng, L. He and W. Huang, *Chem. Soc. Rev.*, 2013, **42**, 622–661.
44 X. Zhang, X. Li, W. Shi and H. Ma, *Chem. Commun.*, 2021, **57**, 8174–8177.